ELECTROSTATIC CHARGE SENSOR BASED ON MICRO RESONATOR WITH SENSING SCHEME OF EFFECTIVE STIFFNESS PERTURBATION

Dongyang Chen, Jiuxuan Zhao, Yinshen Wang, and Jin Xie
The State Key Laboratory of Fluid Power and Mechatronic Systems, Zhejiang University, Hangzhou 310027, People's Republic of China

ABSTRACT

A resonant electrostatic charge sensor with high sensitivity based on micro electromechanical system technology is proposed to measure electric charge. During measurement, input charge produces lateral electrostatic force to change effective stiffness of double-ended tuning forks resonator, and lead to a resonant frequency shift. The charge sensing functionality is experimentally verified and the sensitivity is found to be 4.4×10^{-4} *Hz/fC*^{2}. We show that the proposed scheme has a higher sensitivity compared to the traditional axial strain modulation counterpart. The charge sensing scheme also introduces electrical coupling inside the device to create additional energy transmission path that improve quality factor. The resonant frequency stability associated with linear transduction and instability associated with mechanical nonlinearity are investigated.

INTRODUCTION

Capacitive micro resonator based sensors have been studied for many decades due to IC integration feasibility, revolutionary improvements of small size and low power consumption. A micro resonant electrostatic charge sensor (ECS) can sense small quantity charge with remarkable advantages of large dynamic range and high sensitivity. The ECS has a wide variety of applications, such as aerosol particle detection [1], bio-molecular and electrochemical analysis [2], and isotope ratio measurements [3], etc. The extreme weak charge detection device based on a concept of vibrating-reed capacitors have been reported formerly with a high resolution achieving a level of several electrons [4], nevertheless they suffer from the restriction of intrinsic parasitics due to the complex structure and interface circuit. The weakly coupled resonators based mode localization concept achieves a great sensitivity by virtue of the resonant amplitude variation [5], yet these amplitude modulation devices are short of measurement accuracy compared to the resonant frequency based sensors, and the latter one has a quasi-digital nature of output signal that can be easily fed to the digital readout circuit. Current conventional resonant frequency based charge sense scheme is realized by inputting charge to produce axial electrostatic force to alter effective stiffness of the tines, leading to a resonant frequency shift [6~8]. In attempt to achieve a higher sensitivity, a new resonant frequency based charge sensing scheme, which utilizes input charge to produce lateral electrostatic force to perturb effective stiffness of resonant tines, is firstly introduced in this work. We demonstrate that the resonant frequency variation are more sensitive with external force imposing on the lateral side of tines than the axial direction.

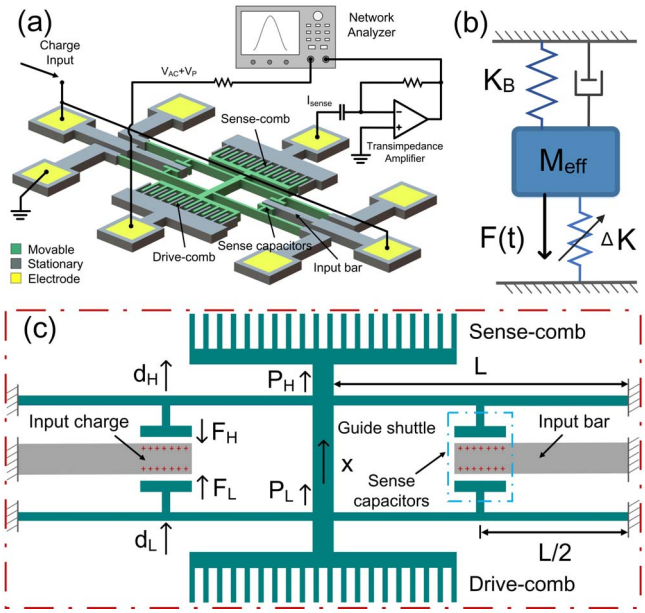

FIG 1: Schematic drawing of (a) the resonant ECS and the experiment setup, (b) the equivalent mass-spring-damper system model and (c) the mechanical model analysis of effective stiffness perturbation of tines.

DESIGN THEORY

The schematic drawing of the resonant ECS is shown in Fig. 1 (a). The device consists of a double-ended tuning forks, a pair of symmetrically distributed interdigitated fingers (IDT) and sense capacitors. A shuttle physically connects both tines at the center to make them mechanically coupled and to vibrate at in-phase mode. The IDTs are chosen to drive the tines into resonance and sense the induced motional current, respectively. Sense capacitor is formed by an input bar parallel placing between two attached plates of tines. The lateral electrostatic attractive forces are generated to act on the attached plates of tines when charge is loaded on the bars. During the resonance of the device, the sense capacitors with input charge function as a nonlinear electrical spring as a result of the gap variation. The effective stiffness perturbation of tines, which is related to the variation of resonant frequency ultimately, is a function of the strength of electrical spring. The equivalent mass-spring-damper system model of the device is shown in Fig. 1 (b), the in-phase mode resonant frequency can be expressed as

$$f_R = \frac{1}{2\pi}\sqrt{\frac{K_B - \Delta K}{M_A + 0.375M}}, \qquad (1)$$

where K_B and ΔK are the mechanical spring constant and the added electrical spring constant of tines, respectively. M and M_A are the masses of tines and its attached loads, respectively. The mechanical model analysis on vibrating tines is shown in Fig. 1 (c). Charge will redistribute on the bars due to the gap change during resonance to keep an equilibrium potential difference across sense capacitors. Due to the four sense capacitors are parallel connected, the potential difference can be given by

$$U = \frac{Q}{C_T} = \frac{Q}{2\times[\varepsilon A/(g-d_L) + \varepsilon A/(g+d_H)]}, \quad (2)$$

where Q denotes the total input charge on both bars. C_T is the total capacitance of sense capacitors. g and A are the initial gap distance and the plate area of sense capacitor, respectively. ε is the dielectric constant. d_L and d_H are the vibration displacement at midpoint of the underneath and upside beams, respectively. And the force at those points, F_L and F_H, can be expressed as the electrostatic attractive force inside the sense capacitors, respectively, shown as

$$F_{L,H} = \frac{\varepsilon A U^2}{2\times(g \mp d_{L,H})^2}. \quad (3)$$

Euler-Bernoulli beam equations with boundary conditions of clamped-guided beam, and Castigliano's theorem with situation of small displacement on a linear elastic body [9, 10], are used to solve the small displacement at the midpoint of underneath and upside beams, respectively. Both the small displacement are deduced as

$$d_{L,H} = \frac{\pm F_{L,H} L^3}{192EI} + \frac{x}{2}, \quad (4)$$

where x is the deflection at the guided-end of beams. E and I are the Young's modulus of elasticity and the moment of inertia, respectively. L is the length of beam. Considering the deflection stiffness and the electrostatic force at the mid-point of beams, the reaction force at the guided-end of both underneath and upside beams can be respectively determined by

$$P_{L,H} = \frac{12EIx}{L^3} \mp \frac{F_{L,H}}{2}. \quad (5)$$

Accordingly, the effective stiffness of tines can be deduced from the total reaction force of four guided-end versus their displacement. Combining the above equations we can get

$$K_{eff} = \frac{2(P_L + P_H)}{x} \approx \frac{48EI}{L^3} - \frac{Q^2}{16\varepsilon Ag}. \quad (6)$$

The first term of equation is known as the mechanical spring constant K_B of guided beams and the second term is the perturbed stiffness ΔK of tines. The perturbed stiffness has a quadratic relationship with input charge, and the value is mainly determined by the design of initial gap and plate area of sense capacitor. Substituting equation (6) to equation (1), and then expanding into Taylor series, the frequency shift can be obtained as

$$\Delta f = f_N \frac{Q^2 L^3}{128\varepsilon gAEWt^3}, \quad (7)$$

where f_N is the natural frequency of tines. W and t are the width and thickness of tines, respectively. Therefore the sensitivity can be expressed as

$$S_L = \frac{\Delta f}{Q^2} = \frac{f_N L^3}{128\varepsilon gAEW^3 t}. \quad (8)$$

Accordingly the theoretical sensitivity of the device is calculated to be $3.6\times10^{-4} Hz/fC^2$ with the design parameters. The sensitivity is dominated by the dimensions of sense capacitor and tines. Optimizing the structure such as increasing the width length ratio W/L or decreasing the plate area A can realize a better sensitivity.

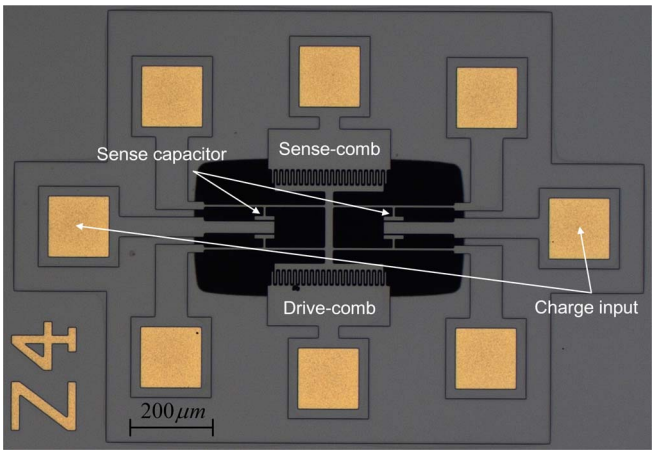

FIG 2: Optical micrograph of the fabricated resonant ECS.

EXPERIMENT RESULTS

The optical micrograph of the fabricated resonant ECS is shown in Fig. 2, the device has a dimension of 1500μm in length and 1000μm in width. And the fabrication is realized through a commercial SOIMUMPs foundry process from MEMSCAP. The experimental measurement setup of the device is illustrated in Fig. 1 (a). The device has been placed in a custom vacuum chamber with an air pressure lever under 40$mTorr$ at room temperature during experiment. The induced motional current at sense-comb is amplified by a trans-impedance amplifier (FEMTO, DLPCA-200) with a gain of 10^6. The spectral response is recorded by a network analyzer (Agilent E5061B). The movable tines and attached loads are electrically grounded.

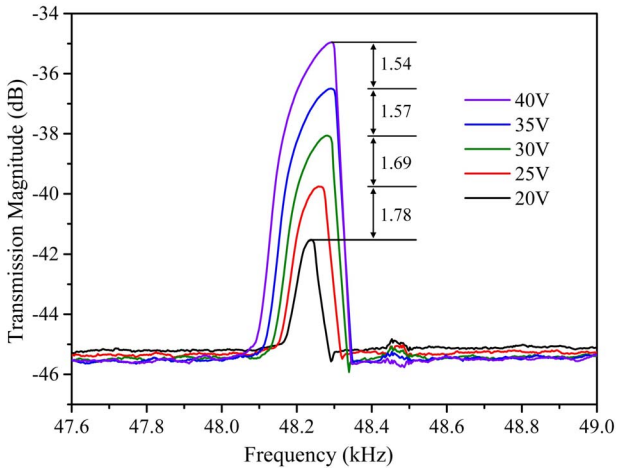

FIG 3: Spectral responses under different polarization voltages with a constant source power of -34dBm.

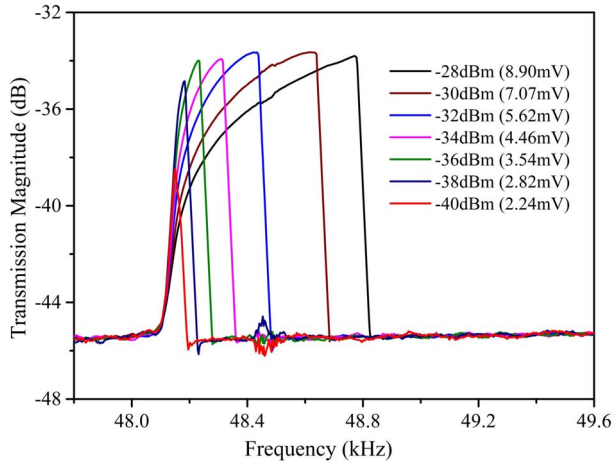

FIG 4: Spectral responses under different source powers with a constant polarization voltage of 30V.

The electromechanical characteristics of resonant ECS has been investigated in the absence of effective stiffness perturbation. The open loop measured in-phase mode spectral responses of the device under the excitation of a series incremental polarization voltages from 15V to 40V with a fixed source power of -34dBm are shown in Fig. 3. The incremental polarization voltages give a linear rise upon corresponding resonant peak, which is attributed to the scarce force dependence on position amid such a drive and sense structure of IDT. And the linear transduction also help to maintain a stable resonant frequency with varied polarization voltage. Fig. 4 plots the spectral responses correspond to a series of incremental source power with constant polarization voltage of 30V. The mechanical nonlinearity caused frequency hysteresis is sensitive with the rising source power, which is associated with strong amplitude-frequency dependence [11]. The open loop measure strategy herein treats the device as a two-port network, thus the equal transmission magnitudes at higher source power region indicating a maximum gain of the resonator. From the characterization we can see that a better signal noise ratio of the output signal can be obtained by adjusting the excitation.

To verify the charge sensing functionality of the device, known quantities of charge are loaded on sense capacitors by applying equivalent step voltage (generated from a DC source-meter, Keithley 2400). Fig. 5 plots the downward resonant frequency shift with increasing input charge while the device is actuated with a polarization voltage of 30V and a source power of -38dBm. An improvement in quality factor with increasing input charge is noticeable, which results from the charge introducing electrical coupling across the sense capacitors, and that creates additional energy transmission path to reduce the energy loss of the device.

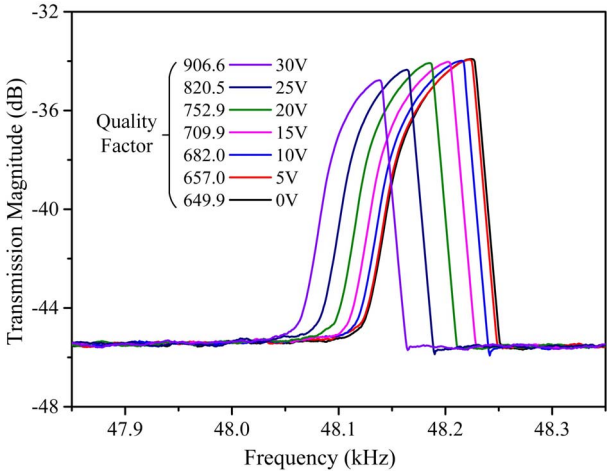

FIG 5: Downward resonant frequency shift of the device while different voltages are applied.

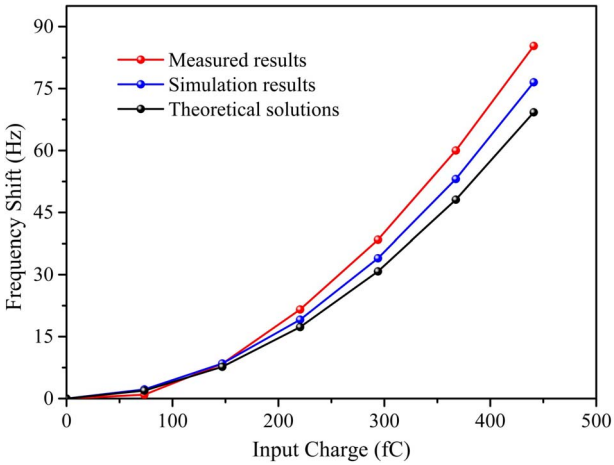

FIG 6: Resonant frequency shift in response to different quantities of input charge.

The quadratic resonant frequency shift in response to different input charge is shown in Fig. 6, as well as the results from theoretical analysis and simulation method. The quadratic polynomial curve fitting is used to determine the sensitivity from analytical, simulated and measured data, respectively, as summarized in table 1. The measured sensitivity is found to be $4.4\times10^{-4}Hz/fC^2$. The analytical sensitivity is agreed well with the simulated one while it has a

deviation within 18.2% compared to measured sensitivity, the dominated inaccuracy is attributed to the fringe effect of sense-comb and the fabrication tolerance.

Table 1: Comparison of results from theoretical analysis, simulation and experiment.

	Resonant frequency (*kHz*)	**Sensitivity (10^{-4}*Hz/fC*^{2})**
Theory	51.17	3.6
Simulation	52.54	3.9
Experiment	48.22	4.5

DISCUSSION

For the charge sensors which resonant frequency shift is caused by the axial strain modulation, the theoretical sensitivity has been given in earlier literatures [6~8]

$$S_A = \frac{\Delta f}{Q^2} = \frac{3 f_N L^2}{80 \varepsilon A E W^3 t}. \quad (9)$$

In order to make a distinct contrast between the presented and previous device, an identical dimensions of both devices is presumed. Substituting equation (9) to (8) we can obtain

$$S_L = \frac{3 f_N L^2}{80 \varepsilon A E W^3 t} \times \frac{80L}{3 \times 128 g} = S_A \times \frac{80L}{3 \times 128 g}. \quad (10)$$

Equation (10) denotes the sensitivity relation between both devices. For the typical design of resonator sensors, the length of tines L has a higher value than the gap of sense capacitor g over two order of magnitude in common, which shows the sensitivity is much greater in the sensing scheme of lateral effective stiffness perturbation compared to axial strain modulation. The measured results herein, the absolute sensitivity of 4.4×10^{-4}*Hz/fC*^{2} and the relative sensitivity of 9.1ppm*/fC*^{2}, also shows a better performance than the formerly reported axial strain modulation type device in the literatures of [6~8], etc.

CONCLUSION

In this work, a high sensitivity resonant ECS with a new sensing scheme of effective stiffness perturbation has been designed, fabricated and tested. Both theoretical and experimental results show a better performance in the proposed device than traditional axial strain modulation counterparts. This charge sensing scheme also has the advantage of improving quality factor by introducing electrical coupling to the device. Besides, the performance further improvement of the device can be realized by introducing force amplification of mechanical leverage [7, 8] or embedding the device into an oscillation loop [12].

ACKNOWLEDGEMENTS

This work is supported by the "National Natural Science Foundation of China (51475423)", the "Zhejiang Provincial Natural Science Foundation of China (No.: LY14E050018)" and the "Science Fund for Creative Research Groups of National Natural Science Foundation of China (No.: 51521064)".

REFERENCE

[1] J. Gerardo, C. Buffa, M. Li, F. Brechtel, G. Langfelder, D. Horsley. "MEMS electrometer with femtoampere resolution for aerosol particulate measurements." *IEEE Sensors Journal*, vol 13, pp. 2993-3000, 2013.

[2] A. Menzel, A. Lin, P. Estrela, P. Li, A. Seshia. "Biomolecular and electrochemical charge detection by a micromechanical electrometer". *Sensors and Actuators B: Chemical*, vol. 160, pp. 301-305, 2011.

[3] T. Ireland, N. Schram, P. Holden, et al. "Charge-mode electrometer measurements of S-isotopic compositions on SHRIMP-SI". *International Journal of Mass Spectrometry*, vol. 359, pp. 26-37, 2014.

[4] J. Lee, Y. Zhu, A. Seshia. "Room temperature electrometry with SUB-10 electron charge resolution". *Journal of Micromechanics and Microengineering*, vol. 18, pp. 025033, 2008.

[5] Ch. Zhao, M. Montaseri, G. Wood, et al. "A review on coupled MEMS resonators for sensing applications utilizing mode localization". *Sensors and Actuators A: Physical*, vol. 249, pp. 93-111, 2016.

[6] J. Lee, B. Bahreyni, A. Seshia. "An axial strain modulated double-ended tuning fork electrometer". *Sensors and Actuators A: Physical*, vol. 148, pp. 395-400, 2008.

[7] J. Zhao, H. Ding, J. Xie. "Electrostatic charge sensor based on a micromachined resonator with dual micro-levers". *Applied Physics Letters*, vol. 106, pp. 233505, 2015.

[8] D. Chen, J. Zhao, Z. Xu, J. Xie. "A micro resonant charge sensor with enhanced sensitivity based on differential sensing scheme and leverage mechanisms". *AIP Advances*, vol. 6, pp. 105106, 2016.

[9] M. Manav, G. Reynen, M. Sharma, E. Cretu, A. Phani. "Ultrasensitive resonant MEMS transducers with tuneable coupling". *Journal of Micromechanics and Microengineering*, vol. 24, pp. 055005, 2014.

[10] J.C. McCormac, R.E. Elling, *Structural analysis*, New York: Harper & Row, 1984.

[11] M. Agarwal, H. Mehta, R. Candler, et al. "Scaling of amplitude frequency dependence nonlinearities in electrostatically transduced microresonators". *Journal of Applied Physics*, vol. 102, pp. 074903, 2007.

[12] S. Sonmezoglu, M. Li, D. Horsley. "Force-rebalanced Lorentz force magnetometer based on a micromachined oscillator". *Applied Physics Letters*, vol. 106, pp. 093504, 2015.

CONTACT

*Jin Xie. tel: +86-571-87952274; xiejin@zju.edu.com